

# Study on the Hydroconversion Law of Coal-Based Heavy Fractions with Different Catalyst Contents Based on an Improved Separation Method

Yi Wang, Feng Tian, Yonghong Zhu, Louwei Cui, Xiaoyong Fan, Chongpeng Du, Feili Wang, Huaan Zheng, Yang Yang\* and Dong Li\*



Cite This: *ACS Omega* 2023, 8, 22440–22452



Read Online

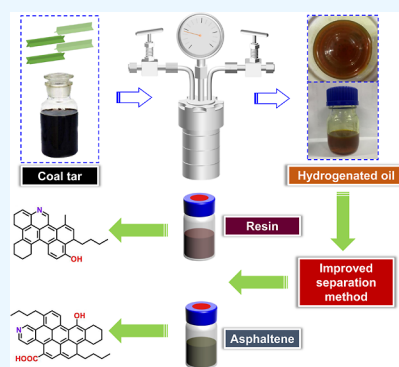
ACCESS |

Metrics & More

Article Recommendations

Supporting Information

**ABSTRACT:** Heavy fractions (e.g., asphaltene and resin) can easily be subjected to physical aggregation and chemical coking reaction through molecular force in the process of lightweight processing and use of coal tar (CT), such that the normal processing and use can be affected. In this study, hydrogenation experiments were performed by regulating the catalyst to oil ratio (COR), while the heavy fractions of the hydrogenated products were extracted based on a novel separation method (e.g., the resin with a poor separation effect and rare existing research). The samples were analyzed through Fourier transform infrared spectroscopy, X-ray photoelectron spectroscopy, nuclear magnetic resonance spectroscopy, and thermogravimetric analysis. On that basis, the composition and structure characteristics of heavy fractions and the law of hydrogenation conversion were investigated. As indicated by the results, with the rise of the COR, the saturates, aromatics, resins, and asphaltenes (SARA) contents indicated the law of increasing the content of saturate, decreasing the content of other fractions, as well as sharply decreasing the content of asphaltene. Moreover, with the increase of the reaction condition, the relative molecular weight, the content of the hydrogen bonded functional groups and C–O groups, the carbon skeleton properties, the number of aromatic rings, and the stacking structure parameters were progressively reduced. In comparison with resin, asphaltene was characterized by large aromaticity and more aromatic rings, short and less alkyl side chains, as well as more complex heteroatoms on the surface of the heavy fractions. The results achieved in this study are expected to lay a solid basis for the relevant theoretical research and facilitate the industrial use process of CT processing.



## 1. INTRODUCTION

Currently, global crude oil reserves have been continuously reduced, and a growing stress is placed on heavy quality and inferior quality, and several national policies have been promulgated (e.g., “carbon peaking and carbon neutralization”). Under the present context, environmental protection regulations turn out to be progressively stringent, and relevant industries are subjected to urgent problems (e.g., green, clean, and sustainable development).<sup>1</sup> Given a considerable number of issues in crude oil processing, scholars have suggested that the use of heavy oil resources (e.g., vacuum residue, oil sand, shale oil, and coal tar) has become more frequent and taken on critical significance.<sup>2–5</sup> Among numerous heavy oils, coal tar, i.e., a liquid by-product in the coal pyrolysis process, exhibits a significantly complex composition and structure. The direct combustion of coal tar as a fuel can impose incalculable harm to the environment while wasting the high value-added products in coal tar. Hydrolighting technology is capable of effectively converting heavy oil products (e.g., coal tar) into high-quality light oil, and it has served as a critical technology for cleanly and efficiently converting and using heavy oil.<sup>6</sup> Furthermore, carbon technology has developed

rapidly, and needle coke can be synthesized as a heavy oil-based battery anode material.<sup>7</sup>

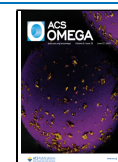
However, existing research<sup>8–10</sup> has suggested that considerable heavy fractions in coal tar (e.g., asphaltene and resin) are easy to produce aggregates or trigger free radical reaction through molecular force for their highly condensed and multi heteroatom structure. As a result, heavy fractions are incompletely converted into light components in the processing process. Furthermore, there are problems (e.g., catalyst poisoning and deactivation, coking and blocking equipment), such that the quality and storage stability of oil products can be adversely affected.

Extensive research has suggested that the asphaltene and resin structures in coal tar are similar to those in petroleum,

Received: January 3, 2023

Accepted: June 5, 2023

Published: June 15, 2023



i.e., they refer to substances that cover polycyclic aromatic hydrocarbons as the main body, where a certain amount of alkyl side chains and more organic heteroatoms are attached.<sup>11</sup> Numerous scholars have investigated the composition and structure of heavy fractions in depth through chemical characterization. Rodgers's team systematically clarified the composition, judgment basis, and solubility of the island/archipelago structure of asphaltene through Fourier transform ion cyclotron resonance mass spectrometry (FT-ICR MS) and other characterization methods.<sup>12–15</sup> Zhu et al.<sup>16,17</sup> systematically investigated the distribution of nitrogen-containing compounds and oxygen-containing compounds in aromatic, resin, and asphaltene in coal tar by comprehensive two-dimensional (2D) gas chromatography and time of flight mass spectrometer (GC × GC-TOF MS) and FT-ICR MS, respectively. Furthermore, their island/island-type structure was analyzed, and the main structure was island-type, as indicated by the result. Moreover, some scholars compared the differences between coal-based and petroleum-based heavy fractions. Weiping et al.<sup>18</sup> studied coal-based and petroleum-based asphaltene through FT-ICR MS with two different ionization modes and found that the molecular weight of coal-based asphaltene is less than petroleum-based, whereas the relative abundance and complexity of oxygenates are higher than those in petroleum. Zhu et al.<sup>19</sup> proposed a novel efficient SARA separation method to extract asphaltene and resin in coal tar and vacuum residue and studied the differences of samples through FT-IR, XPS, NMR, and TG. Existing research has suggested that coal-based heavy fractions contain more oxygen atoms and hydrogen bond groups than petroleum-based ones, and their aromatic rings have a higher degree of condensation.

Numerous scholars have performed relevant research on the changes of asphaltene composition and structure before and after hydrogenation under different process conditions. Morawski's and Mosio-Mosiewski<sup>20,21</sup> used the Ni–Mo/Al<sub>2</sub>O<sub>3</sub> catalyst to investigate the effect of process parameters on the chemical composition change of vacuum residue and asphaltene conversion behavior under the temperature of 410–450 °C, the pressure of 12–20 MPa, the liquid hourly space velocity of 0.25–0.75 h<sup>-1</sup>, and the catalyst ratio of 1–10 wt %. Pei et al.<sup>22</sup> performed hydrofining experiments on coal tar in a trickle bed hydrogenation reactor and analyzed the effects of different reaction temperatures (350–410 °C) on asphaltene composition and structure through X-ray diffraction (XRD), XPS, FT-IR, and NMR. Besides, Shao et al.<sup>23</sup> used a trickle bed hydrogenation reactor to study the effect of different reaction pressures (6–12 MPa) on the composition and structure of asphaltene. In addition, other scholars have advanced relevant research, in which Jin et al.<sup>24</sup> added tetralin as a hydrogen-donating solvent to the residue hydrogenation system, which significantly inhibited the coking reaction of the residue. Wang et al.<sup>25</sup> explored the reactivity of the modified HZSM-5 catalyst to hydrogenate coal tar asphaltene pyrolysis products into benzene-toluene-xylene and naphthalene.

In brief, the asphaltene and resin in hydrogenated oil at different CORs were extracted efficiently and scientifically using the novel SARA separation method of coal tar. The chemical composition and microstructure characteristics of the heavy fractions in coal tar and hydrogenated oil were analyzed systematically based on FT-IR, XPS, NMR, and TG. On that basis, the law of hydrogenation and conversion of heavy

fractions can be determined, and even a theoretical reference and support can be provided for its light use process.

## 2. MATERIALS AND METHODS

**2.1. Materials.** This study was performed based on Zhu et al.<sup>19</sup> The coal tar sample was produced through the coal pyrolysis process at 600 °C in Shenmu City, Shaanxi Province, China. The basic properties of the raw materials are illustrated in our previous research.<sup>26</sup> Table 1 lists the properties of coal

**Table 1. Basic Physical and Chemical Properties of Coal Tar**

property	unit	value	property	unit	value
density, 20 °C	g·cm <sup>-3</sup>	1.05	carbon residue	wt %	6.79
viscosity, 50 °C	mm <sup>2</sup> ·s <sup>-1</sup>	19.31	ash yield	wt %	0.12
Distillation Range			Elemental Analysis		
IBP	°C	155	C	wt %	82.76
5%/10%	°C	196/236	H	wt %	8.27
30%/50%	°C	291/361	O <sup>a</sup>	wt %	7.75
70%/90%	°C	391/475	N	wt %	0.97
FBP	°C	543	S	wt %	0.25

<sup>a</sup>Calculated by difference.

tar. Hydrogenation series catalysts comprised hydrodesulfurization (HDS) catalyst and hydrodenitrogenation (HDN) catalyst. Table 2 lists the basic physical and chemical properties of the catalysts.

**Table 2. Basic Physical and Chemical Properties of Hydrogenation Catalyst**

type	specific surface area (m <sup>2</sup> ·g <sup>-1</sup> )	bulk density (g·mL <sup>-1</sup> )	pore volume (mL·g <sup>-1</sup> )	active metal	carrier
HDS	258	0.81	0.32	Ni–Mo	γ-Al <sub>2</sub> O <sub>3</sub>
HDN	235	0.76	0.36	Ni–Mo–W	γ-Al <sub>2</sub> O <sub>3</sub>

**2.2. Experimental Procedure.** At the early stage, a method suitable for the separation of coal tar fractions was developed, leading to the significantly increased yield of the traditional petrochemical industry standard<sup>27</sup> method from 78% to nearly 98%. Notably, the separation effect of heavy fractions, the core of this study, was greatly improved, i.e., asphaltene was purified, and the yield of resin was increased sharply. Based on the new separation method,<sup>19</sup> dry pre sulfuration was first adopted, CS<sub>2</sub> served as sulfuration agent, and the two hydrogenation series catalysts were changed from oxidation state to sulfuration state through tubular furnace. They were kept at constant temperature of 230 and 280 °C for 3 h, at 320 and 360 °C for 4 h. Next, the hydrogenation experiments were performed in the reactor kettle under the conditions of reaction temperature of 370 °C, reaction time of 90 min, initial hydrogen pressure of 10 MPa, and different COR (1:25, 1:20, 1:15, and 1:10). Lastly, the heavy fractions of hydrogenated oil were extracted.

**2.3. Analytical Methods.** **2.3.1. Elemental Analysis.** The heavy fractions in coal tar (CTHF) and in hydrogenated product oil were primarily analyzed using a wide variety of characterization methods. Elemental analysis (EA) was performed by a Vario EL cube element analyzer of German ELEMENT company, including the contents of C, H, N, and S.

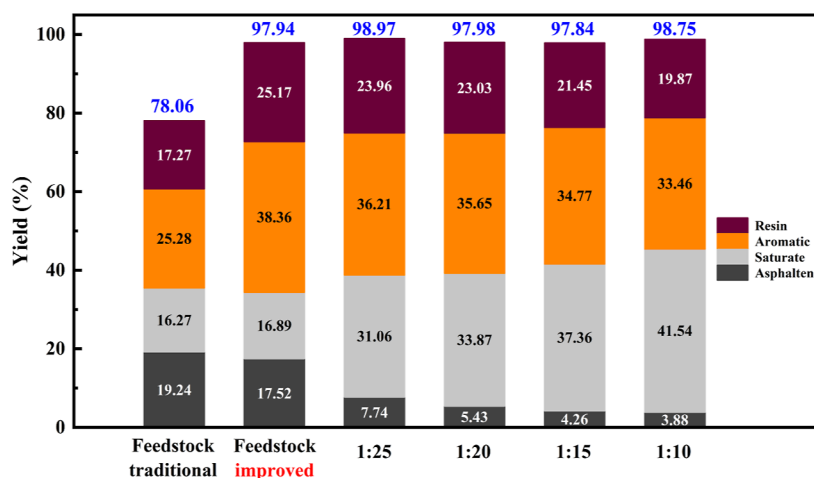


Figure 1. SARA distribution of feedstock and hydrogenated oil at different COR.

Table 3. Elemental and Molecular Weight Analysis of Heavy Fractions of Feedstock and Product Oil

sample	COR	elemental analysis (wt %)					$M_w$	average molecular formula
		C	H	O	N	S		
AS	CTHF	80.61	5.64	11.55	1.92	0.29	630	$C_{42.32}H_{35.53}O_{4.55}N_{0.86}S_{0.06}$
	1:25	82.45	5.94	9.60	1.73	0.28	598	$C_{41.09}H_{35.52}O_{3.59}N_{0.74}S_{0.05}$
	1:20	83.37	6.42	8.29	1.65	0.27	576	$C_{40.02}H_{36.98}O_{2.98}N_{0.68}S_{0.05}$
	1:15	84.09	6.75	7.37	1.54	0.25	559	$C_{39.17}H_{37.73}O_{2.57}N_{0.61}S_{0.04}$
	1:10	84.82	7.23	6.25	1.46	0.24	542	$C_{38.31}H_{39.19}O_{2.12}N_{0.57}S_{0.04}$
RE	CTHF	82.33	6.18	9.80	1.42	0.27	496	$C_{34.03}H_{30.65}O_{3.04}N_{0.50}S_{0.04}$
	1:25	83.93	6.48	7.97	1.37	0.25	458	$C_{32.03}H_{29.68}O_{2.28}N_{0.45}S_{0.04}$
	1:20	84.58	6.96	6.98	1.24	0.24	443	$C_{31.22}H_{30.83}O_{1.93}N_{0.39}S_{0.03}$
	1:15	85.61	7.41	5.63	1.13	0.22	435	$C_{31.03}H_{32.23}O_{1.53}N_{0.35}S_{0.03}$
	1:10	86.27	7.76	4.74	1.02	0.21	426	$C_{30.63}H_{33.06}O_{1.26}N_{0.31}S_{0.03}$

2.3.2. *Gel Permeation Chromatography.* Gel permeation chromatography (GPC) analysis was performed by Ultimate-3000 type gel chromatograph, and the mobile phase was tetrahydrofuran solvent.

2.3.3. *FTIR Analysis.* A Bruker EQUINOX-55 Fourier infrared spectrometer was used for FTIR analysis. KBr was required for tablet pressing before detection. The test condition was the scanning range of 400–4000  $cm^{-1}$ .

2.3.4. *NMR Analysis.* The Varian-FT-80A nuclear magnetic resonance instrument was used for hydrogen nuclear magnetic resonance spectroscopy analysis.  $CDCl_3$  was used as solvent, and tetramethylsilane was selected as the internal standard.

2.3.5. *XPS Analysis.* X-ray photoelectron spectroscopy analysis was performed by a PHI-5400 photoelectron spectrometer of PerkinElmer company in the United States, and energy correction was performed with C 1s (284.6 eV) as the standard.

2.3.6. *XRD Analysis.* XRD detection was performed with a D/MAX-2400 X-ray diffractometer from Rigaku Corporation, at a scan rate of  $8^\circ/min$ , under a  $2\theta$  scan range of  $5-80^\circ$ , and  $\lambda = 0.15406$  nm. The apparent microcrystalline structure parameters were determined in accordance with the Scherrer and Bragg equation,<sup>22,23</sup> comprising inter aromatic layer distance ( $d_m$ ), aliphatic or naphthenic chain layer distance ( $d_\gamma$ ), average diameter of aromatic sheet ( $L_a$ ), average stack height of aromatic sheet ( $L_c$ ), average number of aromatic sheets associated in per stacked cluster ( $M_c$ ), and average aromatic ring number per sheet ( $R_a$ ).

### 3. RESULTS AND DISCUSSION

3.1. *Fractions Distribution of Hydrogenation Products.* According to the improved separation method, the SARA of the hydrogenation product at different CORs were separated, and the content distribution is shown in Figure 1. Coal tar hydrogenation is a gas–liquid–solid three-phase catalytic reaction process.  $H_2$  first dissolves in the liquid phase and then diffuses to the active center on the catalyst surface to generate active hydrogen to participate in the chemical reaction. As depicted in Figure 1, with the increase of the amount of catalyst added, the catalytic active sites in the system were increased, such that the light conversion of heavy fractions was facilitated, and the asphaltenes content declined rapidly from 17.52% in the feedstock to 3.88%, which was transformed into aromatic ring structural substances (e.g., resin). Moreover, the primary resins were converted into aromatic and saturate fractions though some primary asphaltenes were converted into resins. Accordingly, the contents of resins and aromatics declined, suggesting that the conversion rate of asphaltenes converted into resins was lower than the rate of resins converted into aromatic and saturate fractions. Furthermore, the content of saturate was increased sharply from 16.89% in the feedstock to 41.54% due to the hydrogenation and saturation reaction of the other fractions.

The conversion efficiency of asphaltene has been reported as one of the critical factors for the catalytic hydrogenation of coal tar. After calculation, when the value of the COR was increased, the conversion rate of asphaltene in the product oil was increased significantly from 55.82 to 77.85%. When the

value of the COR reached a certain degree, the rise of its value cannot lead to the significantly increased conversion rate of asphaltene. The reason for the result is that the catalyst in the hydrogenation system can promote the reaction, and it is also the center of coke formation. This is easy to lead to the condensation reaction of resin and convert it into asphaltene again. Moreover, an excessive amount of the catalyst is prone to aggregation and sedimentation. Therefore, the total specific surface area of the catalyst and reduces the contact area between the catalyst and  $H_2$  can be reduced. As a result, the catalytic conversion efficiency will decline.

**3.2. EA & GPC Analyses.** In accordance with EA and GPC, the organic element content and relative molecular weight ( $M_w$ ) of heavy fractions in feedstock and product oil at different CORs were obtained, as listed in Table 3. With the increase of the COR, the active sites in the catalyst system were increased, such that the progress of the aromatic ring saturation reaction and the heteroatom removal reaction can be facilitated. This will increase the degree of lightning of the heavy fractions. The content of carbon and hydrogen in the heavy fractions of the product oil increased significantly, while the content of heteroatoms was apparently reduced by the conversion of heteroatoms into corresponding hydrides through hydrogenolysis reaction. The  $M_w$  of asphaltenes tended to decline from 630 to 542, and the resins were reduced from 496 to 426. Furthermore, the H/C of asphaltene was increased from 0.84 to 1.02 in the feedstock, and the H/C of resin was slightly increased from 0.90 to 1.08, further confirming the occurrence of lightweight processing.

Heteroatom organic compounds with an aromatic ring structure are very difficult to remove, so the removal rate of heteroatom is often used as one of the evaluation methods to investigate the hydrogenation effect. Figure 2 presents the removal rate of heteroatoms of heavy fractions at different CORs. As depicted in Figure 2, the contents of three organic heteroatoms in heavy fractions declined with the increase of the COR, such that their removal rate tended to be elevated. An oxygen atom is characterized by lower structural complexity and higher reaction activity over sulfur atom and nitrogen

atom with an aromatic ring structure, such that the removal rate turned out to be higher at the respective investigation point. Under the effect of the lower condensation degree of the condensed aromatic hydrocarbon structure, the three elements achieved higher removal rates than those in asphaltene. Moreover, with the elevation of the COR, the nitrogen atom removal rate in asphaltene was increased from 9.90 to 23.96%, and the nitrogen atom in resin displayed an increase from 3.52 to 28.17%. In contrast, the nitrogen removal rate in petroleum was generally 40%.<sup>28,29</sup> Moreover, the removal rate of sulfur atom in asphaltene was elevated from 3.45 to 17.24%, and that in resin, it was increased notably from 7.41 to 22.22%. In comparison, the removal rate of sulfur in oil generally reached 70%.<sup>28,30</sup> The removal effect of the two heteroatoms in heavy fractions of coal tar was lower than that in petroleum. The major reason for the above result is that coal-based asphaltenes cover more thiophene sulfur, pyridine ring, and other compounds with aromatic ring structure over petroleum-based ones. The above-mentioned compounds should be saturated with aromatic rings prior to the complete hydrogenation of heterocycles. Likewise, with the increase of the COR, the reaction degree was limited, and the increase of the removal rate of sulfur and nitrogen atoms in heavy fractions was inhibited to a certain extent.

**3.3. FT-IR Analysis.** The relative absorption intensity and the position of the absorption band in the FT-IR spectra can indicate the composition of functional groups, the bonding between functional groups, and their vibrational properties of the sample.<sup>31</sup> Compared with the attribution results of characteristic absorption peaks generally involved in the analysis of coal tar and petroleum,<sup>32,33</sup> the FT-IR spectra fell into four regions, i.e., hydrogen bond region (I: 3650–3100  $cm^{-1}$ ), aliphatic C–H stretching vibration region (II: 3000–2800  $cm^{-1}$ ), C–O region (III: 1800–1000  $cm^{-1}$ ), and aromatic C–H bending vibration region (IV: 900–600  $cm^{-1}$ ),<sup>34</sup> to investigate the functional group structure of the sample in depth. Figure 3 presents the FT-IR spectra of heavy fractions at different CORs.

In the range of the hydrogen bond region, –OH stretching vibration absorption peak and N–H bond vibration absorption peak were identified, which can easily lead to the correlation of heavy fractions.<sup>35</sup> Compared with the result in feedstock,<sup>19</sup> the absorption intensity of the heavy fractions after hydrogenation in this area declined, and this trend turned out to be more significant with the increase of the COR, suggesting that the hydrogen bond groups of heavy fractions were removed more significantly with the increase of the COR. As revealed by the comparison of the similarities and differences between asphaltene and resin, the intensity and width of the characteristic absorption peaks of asphaltenes in this region were larger than those of resin, such that asphaltene aggregated, and micelles were formed, affecting the processing and use of coal tar.<sup>36</sup> Although the properties of resin are basically consistent with those of asphaltenes, they have a low degree of condensation and cannot self-aggregate while only aggregating with asphaltenes through bridging bonds (e.g., hydrogen bonding of heteroatom functional groups).<sup>37</sup>

In the C–H stretching vibration region of aliphatic, the heavy fractions displayed absorption peaks under a range of working conditions. Their intensity and content tended to be reduced with the increase of the COR, suggesting the occurrence of lightweight reactions of heavy fractions (e.g., aromatic ring hydrogenation saturation, cycloalkyl ring open-

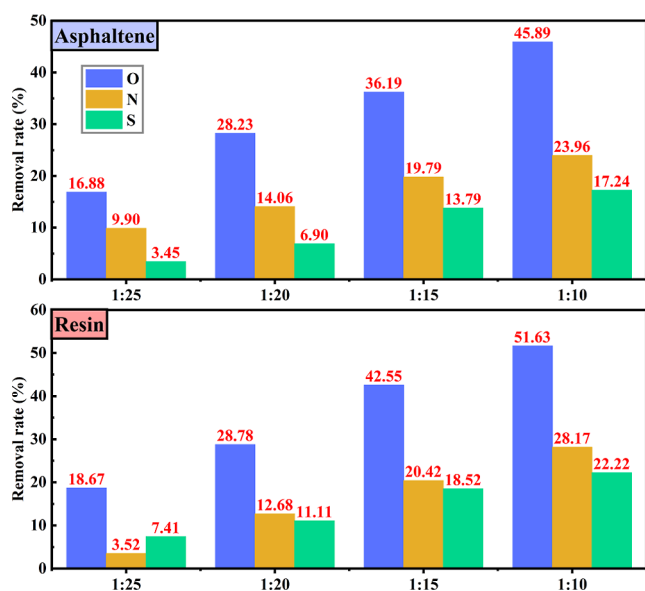
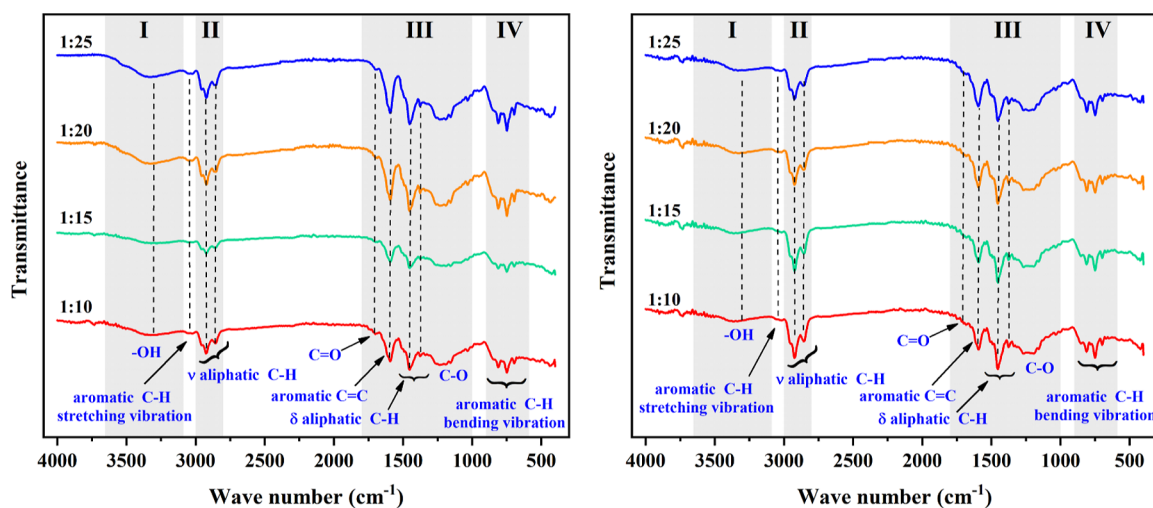
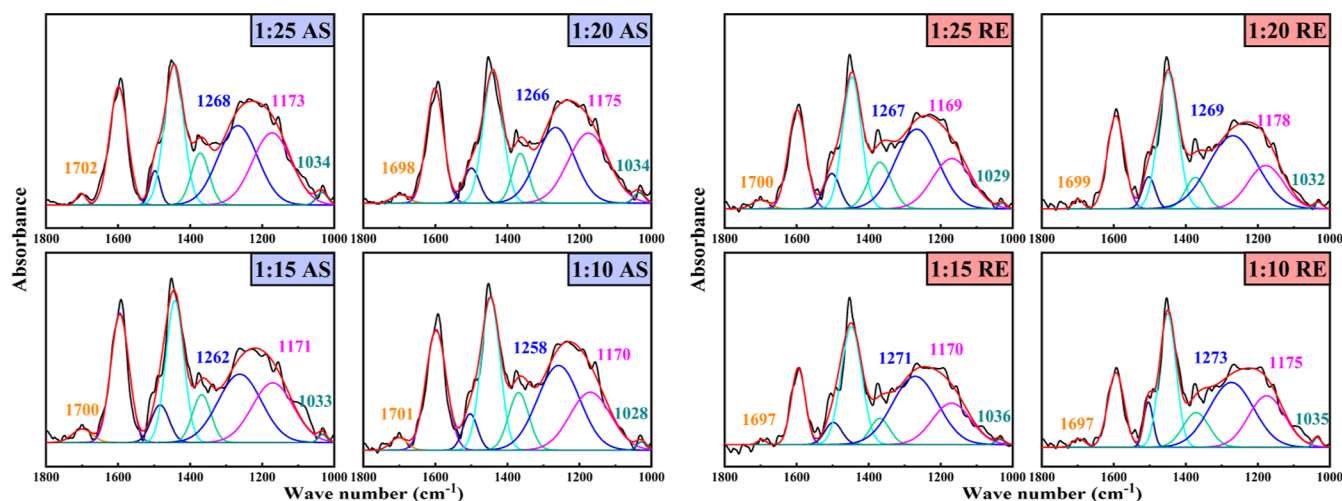


Figure 2. Removal rate of heteroatoms of heavy fractions at different CORs.



**Figure 3.** FT-IR spectra and peak separation for C–O region of heavy fractions at different CORs (the left side represents asphaltene; the right side represents resin).



**Figure 4.** Peak separation of FT-IR for the C–O region of heavy fractions at different CORs (the left side represents asphaltene; the right side represents resin).

**Table 4.** C–O Group Content of Heavy Fractions at Different CORs

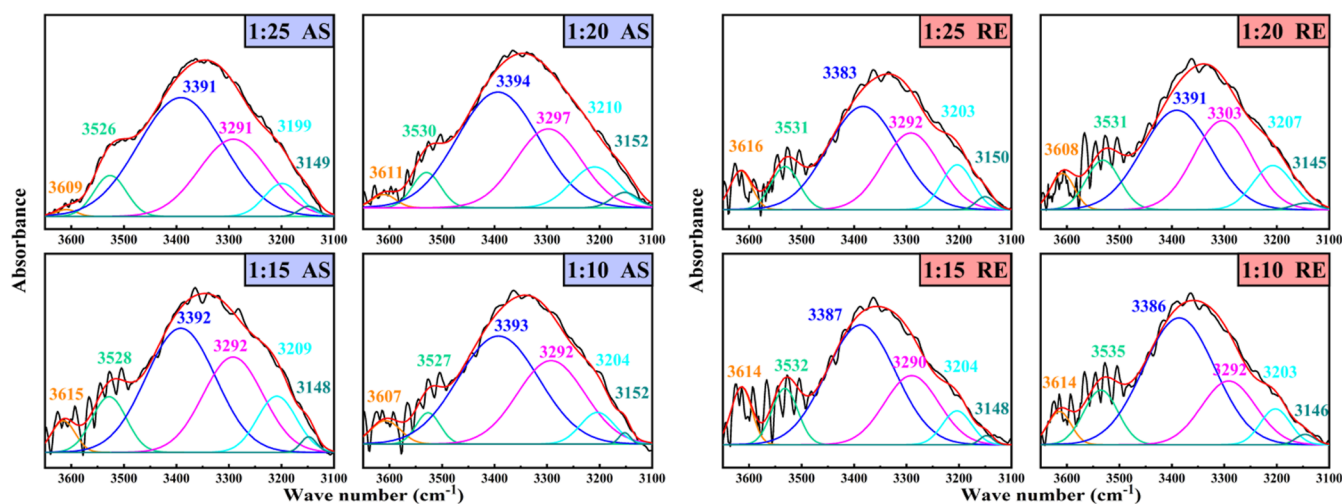
assignment	asphaltene, relative content (%)				resin, relative content (%)			
	1:25	1:20	1:15	1:10	1:25	1:20	1:15	1:10
C=O	1.71	2.37	4.71	3.34	1.78	2.77	2.89	2.11
aromatic ether	54.65	52.29	51.44	52.48	67.98	65.31	62.90	58.35
C–O of phenols	41.41	43.53	42.66	44.97	29.25	31.13	33.24	38.06
C–O–C	2.23	1.80	1.19	1.22	0.99	0.79	0.96	1.47

ing, and C–C bond fracture). Furthermore, compared with resin, asphaltene exhibited a lower absorption peak intensity, such that the structure of asphaltene with a low branching degree can be confirmed.

With the wave number ranging from 1800 to 1000  $\text{cm}^{-1}$ , there existed characteristic peaks of aromatic conjugated double bond C=C structural groups with a wave number of nearly 1620  $\text{cm}^{-1}$  and a variety of C–O groups. Existing research has suggested that<sup>38,39</sup> the region can be fitted by peaks to explore functional group composition in depth. The peak fitting conditions comprised: C=O group with a wave number of nearly 1690  $\text{cm}^{-1}$ , aromatic ether structure with a wave number of approximately 1270  $\text{cm}^{-1}$ , phenolic hydroxyl

with a wave number of about 1180  $\text{cm}^{-1}$ , as well as the ether bond structure with a wave number of nearly 1030  $\text{cm}^{-1}$ . Figure 4 presents the fitting of peaks of C–O region, and the content of the respective structure is listed in Table 4.

As depicted in Table 4, aromatic ethers and phenolic hydroxyl groups accounted for up to 95% of the total amount of C–O bonding, whereas there existed scarce C=O structural groups of carboxylic acid, aldehyde, and ketone. With the increase of the COR, the C–O bonding modes of heavy fractions revealed the law that the content of C=O and phenolic hydroxyl groups is elevated, and the content of aromatic ether groups declines. The compounds with an aromatic ether structure exhibit high reaction activity,<sup>40</sup> and



**Figure 5.** Peak separation for hydrogen bond of heavy fractions at different CORs (the left side represents asphaltene; the right side represents resin).

**Table 5.** Hydrogen Bond Content of Heavy Fractions at Different CORs

assignment	asphaltene, relative content (%)				resin, relative content (%)			
	1:25	1:20	1:15	1:10	1:25	1:20	1:15	1:10
free OH groups	0.76	1.66	3.64	3.86	4.22	4.98	7.23	7.49
OH- $\pi$	7.23	6.46	7.88	5.42	6.96	7.12	6.30	5.39
OH-OH	51.43	50.82	46.51	47.53	52.03	51.07	52.25	51.28
OH-ether O	27.63	28.33	29.40	32.09	26.16	27.20	27.21	29.26
cyclic OH	11.89	11.54	11.32	10.35	9.12	8.64	6.24	5.97
OH-N	1.06	1.19	1.25	0.76	1.51	1.00	0.77	0.61

they can be easily hydrocracked into phenolic compounds, such that the content of aromatic ether can be reduced, and the content of phenolic hydroxyl groups can be increased in the system. As revealed by the higher content of the C=O group and the phenolic hydroxyl group, asphaltene exhibited a more complex C-O condensed structure of polycyclic aromatic hydrocarbons than resin.

As depicted in Table 4, aromatic ethers and phenolic hydroxyl groups accounted for as much as 95% of the total amount of C-O bonding, whereas there were few C=O structural groups of carboxylic acid, aldehyde and ketone. With the increase of the COR, the C-O bonding modes of heavy fractions generally revealed the law that the content of C=O and phenolic hydroxyl groups was increased, and the content of aromatic ether groups declined. The compounds with aromatic ether structure have high reaction activity<sup>40</sup> and are easy to be hydrocracked into phenolic compounds, such that the content of aromatic ether can be reduced, and the content of phenolic hydroxyl groups in the system can be increased. The higher content of C=O group and phenolic hydroxyl group reflects that asphaltene has a more complex C-O condensed structure of polycyclic aromatic hydrocarbons than resin.

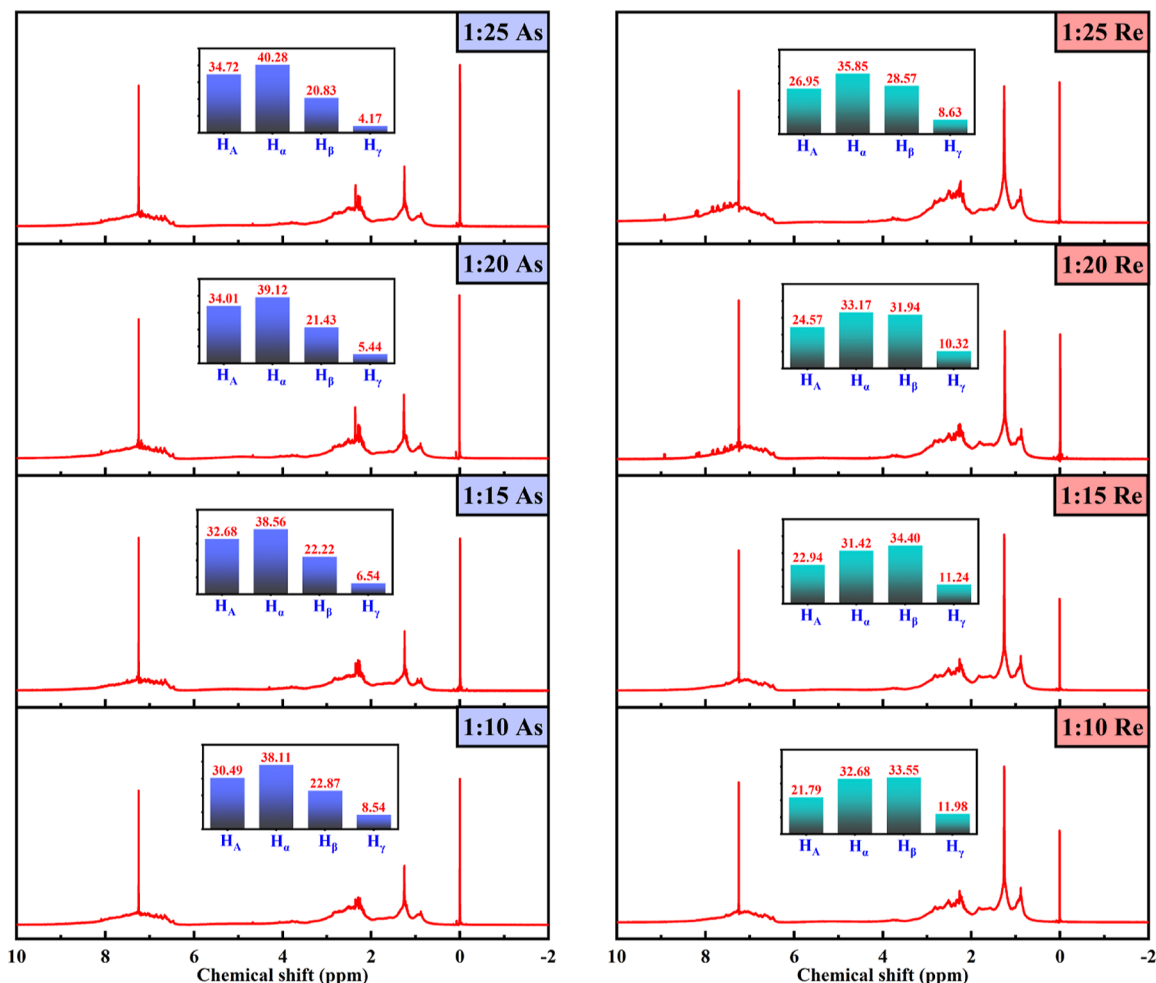
Hydrogen bonding has been confirmed as one of the major functions in the correlation between asphaltene molecular micelles and plays a leading role in the correlation of asphaltene molecular micelles.<sup>41</sup> According to the research,<sup>42</sup> the hydrogen bond regions in the FT-IR spectra of asphaltene and resin can fit by peaks. In accordance with the order of wave number from large to small, the hydrogen bond can be divided into six types. Thus, the hydrogen bond action

between functional groups can be explored. The fitting of peaks is shown in Figure 5, and the content of various types of hydrogen bonds is shown in Table 5.

As depicted in Table 5, the content of the OH-OH type hydrogen bond is the most, accounting for about 50%. In addition, the content of OH-ether O type hydrogen bond was also large, accounting for nearly 25–30%. The content of free OH and OH-N groups was extremely little, especially the OH-N type, almost absent, which was correlated with the acid-base interaction between acidic hydroxyl and alkaline nitrogen atoms. With the increase of the COR, the content of the OH- $\pi$  type hydrogen bond in the system declined, and asphaltene with stronger condensation degree covered more OH- $\pi$  type hydrogen bond than resin. Furthermore, except for free OH, only the content of OH-ether O group increases in the other types of hydrogen bonds, suggesting that other types of hydrogen bonds tend to be transformed into OH-ether O type in the hydrogenation process, in which the content in asphaltene was increased from 27.63 to 32.09%, and that in resin was increased from 26.16 to 29.26%.

**3.4. NMR Analysis.** Refer to the chemical shift interval of four types of hydrogen atoms defined by Xie<sup>43</sup> in NMR spectra, as shown in Figure S1. Figure 6 presents the NMR spectra of asphaltene and resin at different CORs and the relative content of the respective integral interval.

The changes of four types of hydrogen atoms can reflect the progress of catalytic hydrogenation reaction, in which H<sub>A</sub> represents the hydrogen atom in the aromatic ring system, and H <sub>$\omega$</sub> , H <sub>$\beta$</sub> , and H <sub>$\gamma$</sub>  represent the hydrogen atoms at different positions in the alkyl side chain connected by the aromatic ring. The increase of the COR increases the number of active



**Figure 6.** NMR spectra and proportion of the respective integral interval of heavy fractions at different CORs (the left side represents asphaltene; the right side represents resin).

sites in the catalytic system and accelerates the aromatic ring saturation reaction, resulting in the rapid reduction of  $H_A$  hydrogen atoms in the aromatic ring structure in asphaltene and resin, and this value of asphaltene is higher than that of resin, which corresponds to its more complex condensed aromatic ring structure.  $H_\alpha$  in the aromatic side chain system decreases, and  $H_\beta$  and  $H_\gamma$  increase, which reflect that the ring opening reaction and heteroatom hydrogenolysis reaction increase the number and length of alkyl side chains.

According to the results of organic element proportion and relative molecular weight of heavy fractions in Table 3 above and the distribution results of four hydrogen atoms in Figure 6, combined with the modified Brown–Ladner method,<sup>22,23</sup> the average molecular structure parameters of heavy fractions at different CORs, such as aromaticity, number of aromatic rings, number of naphthenic rings, and number of alkyl substitution bases are calculated, which are listed in Table S1.

Comparing the structural parameters of heavy fractions in Table S1, it can be found that the aromaticity ( $f_A$ ) commonly used to judge the degree of molecular condensation gradually decreases with the increase of the COR, and the aromaticity of asphaltene is greater than that of resin, while the aromaticity of asphaltene and resin are reduced from 0.72 to 0.66 and 0.67 to 0.60, respectively. The degree of substitution of the aromatic ring ( $\sigma$ ) is generally used to indicate the degree of aromatic ring branching. As depicted in Table S1, the increase of the

COR led to the increase of  $\sigma$  of heavy fractions, consistent with the increase of alkyl substitution number, and the  $\sigma$  of resin was higher than that of asphaltene, confirming that there were more resin branches and it can be easier to hydrogenate into light fractions (e.g., aromatic components). The increase of the COR led to the decrease of carbon number and heteroatom number in the heavy fractions, in which the  $C_T$  of asphaltene was reduced from 41.09 to 38.31, and the  $C_T$  of resin was reduced from 32.03 to 30.63. Furthermore, the number of aromatic rings and naphthenic rings of heavy fractions declined with the increase of the COR, suggesting that the ring opening rate of the naphthenic ring was greater than that of aromatic ring saturation into the naphthenic ring. Likewise, the number of aromatic rings of asphaltene at the respective inspection point was higher than that of resin, whereas its number of naphthenic rings and alkyl substitution number were not as much as that of resin, further verifying that asphaltene can be a condensed polycyclic aromatic structure with a higher degree of condensation.

**3.5. XPS Analysis.** Qualitative and semi quantitative analyses of the elements at 7 nm of the outer layer of asphaltene and resin can be performed by XPS analysis. The full spectra of asphaltene and resin is shown in Figure S2. The C, O, N, and S elements of the sample were scanned in a narrow area, and the occurrence forms of each element were analyzed qualitatively by Avantage software.<sup>19,44</sup> The peak

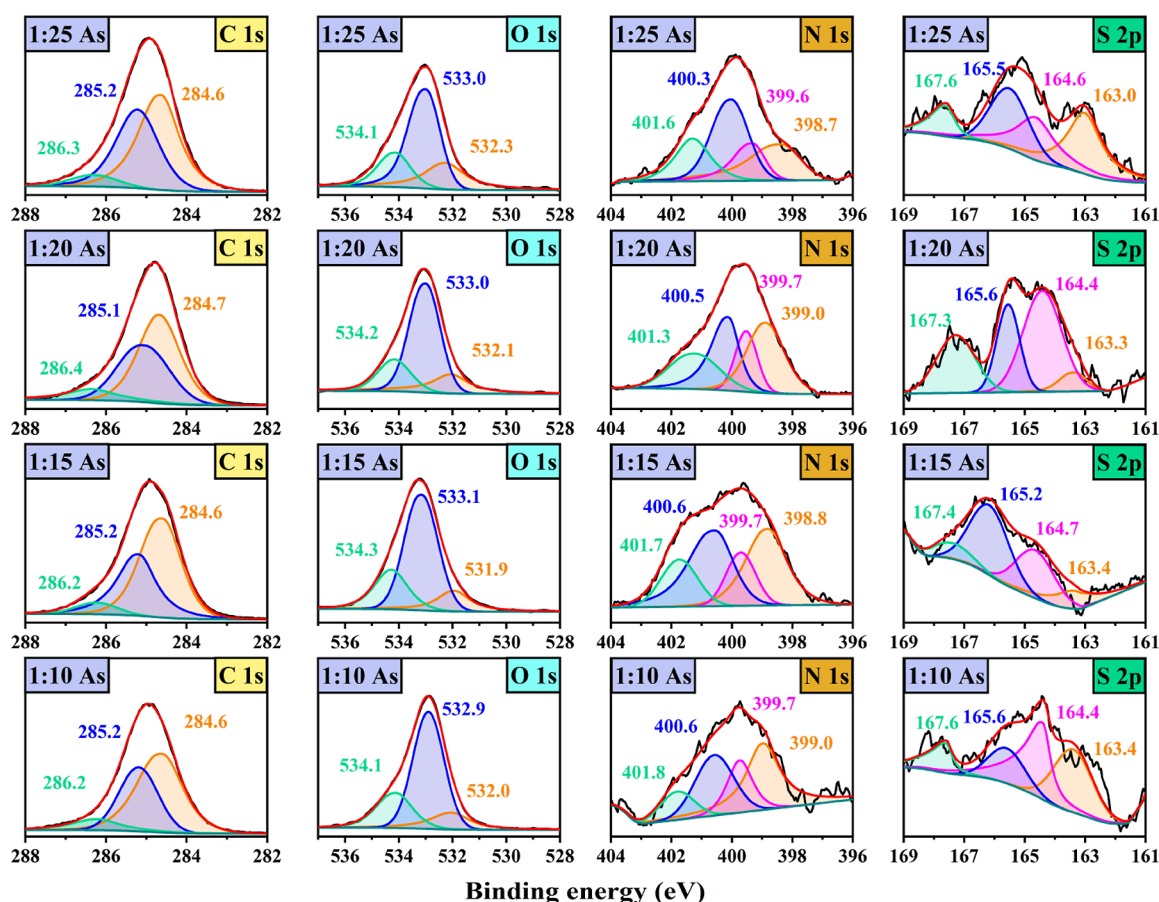


Figure 7. C<sub>1s</sub>, O<sub>1s</sub>, N<sub>1s</sub>, and S<sub>2p</sub> XPS spectra of asphaltene at different CORs.

fitting treatment was performed according to the area normalization method, and the element content was analyzed quantitatively. The peak fitting diagrams of each element in asphaltene and resin at different CORs are shown in Figures 7 and 8, respectively, and the occurrence form results of each element are shown in Table 6.

The main forms of carbon atoms in the heavy fractions of coal tar are  $\pi$ - $\pi$  aromatic carbon structure corresponding to  $sp^2$  hybrid carbon and aliphatic carbon structure corresponding to  $sp^3$  hybrid carbon, which account for about 90% of the whole. In addition, the content of C–O group in asphaltene at any inspection point is slightly higher than that of resin, which corresponds to the higher oxygen content of asphaltene in elemental analysis. The increase of the COR intensifies the hydrogenation saturation of  $sp^2$  hybrid carbon structure to  $sp^3$  aliphatic carbon structure. Thus, the occurrence forms of the above-mentioned two carbon atoms show an opposite trend with the increase of the COR. Geng et al.<sup>45</sup> found that the value of  $sp^2/(sp^2 + sp^3)$  can be used to reflect the aromaticity of heavy fractions, which reflects that the increase of the COR reduces the aromaticity of heavy fractions. In addition, the aromaticity of asphaltene is higher than that of resin, which is consistent with the results of NMR.

The occurrence form of oxygen atoms of asphaltene and resin is mainly compounds with C–O single bond structure (e.g., phenol, ether, and alcohol). The total content of this type is about 50–60%, which is consistent with the fitting result of C–O distinguishing peak in FT-IR, as well as the C–O group in asphaltene is higher than that of resin. The increase of the COR facilitated the hydrogenation saturation of C=O groups

(e.g., carboxylic acid and ketone) into C–OH compounds (e.g., alcohol and phenol).

Aromatic C–N compounds have been confirmed as the major forms of nitrogen atoms (e.g., pyridine and pyrrole), taking up nearly 60–70%. Heterocyclic nitrogen and hydroxyl are capable of forming a significant hydrogen bond and existing in asphaltene as complex, which has been reported as a critical force of asphaltene association.<sup>46</sup> With the rise of the COR, the nitrogen atoms in the aromatic ring structure in asphaltene and resin turn out to be extremely difficult to saturate via the heterocyclic ring for the removal of the C–N bond. Accordingly, the content of this type of nitrogen-containing compounds will not decrease sharply.

The sulfur atoms in heavy fractions can fall into four categories, i.e., alkyl sulfide, thiophene, sulfoxide, and sulfone. However, the regularity is not obvious since the content of sulfur atoms is extremely low and close to the lower detection limit. In general, compared with other types of sulfur-containing compounds, thiophene compounds embedded in the condensed aromatic ring system of asphaltene and resin have been confirmed as the type with the highest occurrence probability of sulfur elements. Affected by its special aromatic ring structure, the C–S bond energy in the structure is significantly strong, the reaction activity is exceedingly low, and it is very difficult to be removed through hydrogenation.

**3.6. XRD Analysis.** The XRD spectra of heavy fractions mainly contain three types of peaks, namely,  $\gamma$  peak, 002 peak, and 100 peak, which are located at  $2\theta$  of 20, 25, and  $43^\circ$ , respectively. The  $\gamma$  peak represents the accumulation of saturated aliphatic hydrocarbons and naphthenic ring



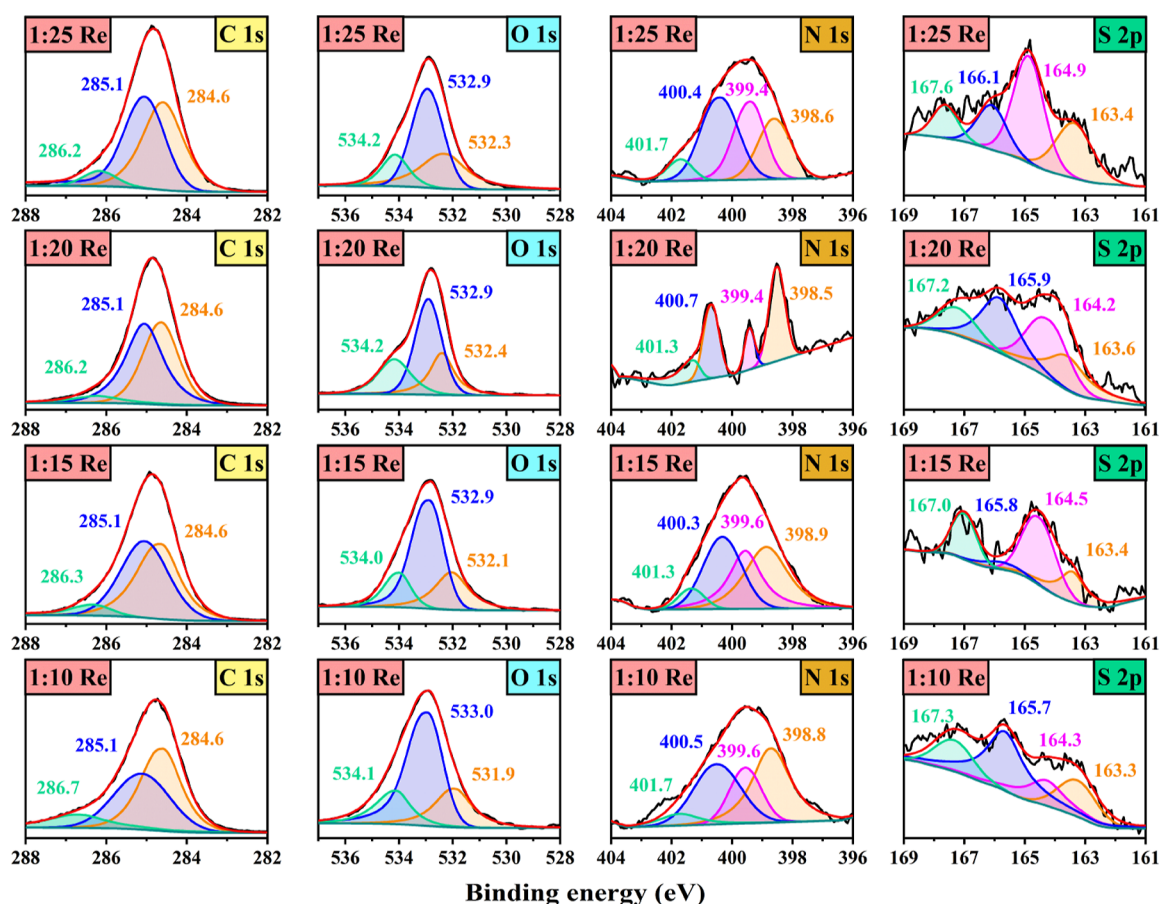


Figure 8. C<sub>1s</sub>, O<sub>1s</sub>, N<sub>1s</sub>, and S<sub>2p</sub> XPS spectra of resin at different CORs.

Table 6. Forms of C, O, N, and S in Heavy Fractions at Different CORs by XPS

element	assignment	asphaltene, relative content (%)				resin, relative content (%)			
		1:25	1:20	1:15	1:10	1:25	1:20	1:15	1:10
C 1s	aromatic C (sp <sup>2</sup> )	54.35	51.55	50.76	50.25	45.87	43.96	42.58	42.27
	aliphatic C (sp <sup>3</sup> )	35.33	39.18	39.09	43.72	41.74	48.31	47.85	51.55
	C–O–C, C–OH, C–O	10.33	9.28	10.15	6.03	12.39	7.73	9.57	6.19
	sp <sup>2</sup> /(sp <sup>2</sup> + sp <sup>3</sup> )	0.61	0.57	0.56	0.53	0.52	0.48	0.47	0.45
O 1s	C=O	24.58	22.73	19.30	18.60	31.58	25.79	24.14	22.29
	C–O–C, C–OH, C–O	55.87	56.82	58.48	58.14	52.63	52.63	57.47	60.24
	COO–	19.55	20.45	22.22	23.26	15.79	21.58	18.39	17.47
N 1s	pyridine-N (N-6)	25.77	32.89	32.62	38.61	24.36	37.31	34.25	38.76
	amino-N	16.15	16.12	15.25	17.37	29.09	17.91	25.68	22.48
	pyrrole-N (N-5)	38.46	31.25	35.46	32.43	36.36	29.10	32.88	32.17
	quaternary-N	19.62	19.74	16.67	11.58	10.18	15.67	7.19	6.59
	(N-5 + N-6)/total N	64.23	64.14	68.09	71.04	60.73	66.42	67.12	70.93
S 2p	alkyl sulphide	31.65	10.30	15.42	32.70	27.31	23.70	25.23	19.91
	thiophene	27.85	42.92	30.40	38.02	44.05	32.47	45.87	19.03
	sulphoxide	30.06	22.32	44.05	17.11	17.62	29.55	5.96	44.25
	sulphone	10.44	24.46	10.13	12.17	11.01	14.29	22.94	16.81

structures, the 002 peak reflects the accumulation of aromatic molecules forming the aromatic layer structure, and the 100 peak represents the average diameter of the aromatic layer.<sup>47</sup> The XRD spectra of heavy fractions at different CORs are shown in Figure 9. The crystallization parameters results are listed in Table 7.

With the increase of the COR, the condensation of heavy fractions was weakened, the size of aromatic core and the spacing of aromatic core group in the condensed aromatic

system were reduced, and the spacing of alkyl chains in the side chain system declined. The above-mentioned law is consistent with the results in Table 7, i.e., the six crystallization parameters tended to be decreased with the increase of the COR. Alkyl substitution chain parameters (i.e.,  $d_m$  and  $d_\gamma$ ) of asphaltenes were less than those of resin, whereas the parameters (i.e.,  $L_a$  and  $R_a$ ) of the polycyclic aromatic hydrocarbon system exceeded those of resin, suggesting that asphaltene can exhibit a higher degree of condensation and

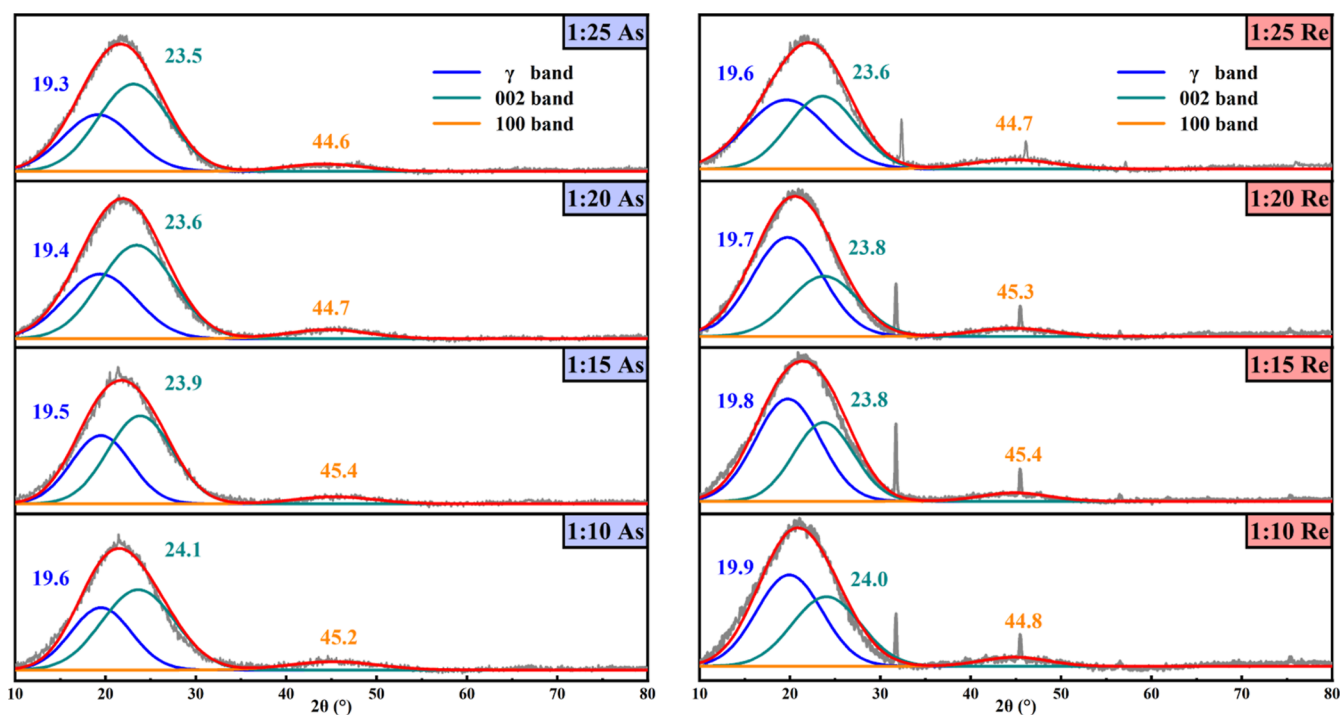


Figure 9. XRD peak fitting diagram of heavy fractions at different CORs (the left side represents asphaltene; the right side represents resin).

Table 7. Crystallization Parameters of Heavy Fractions at Different CORs<sup>a</sup>

crystallization parameters	asphaltene				resin			
	1:25	1:20	1:15	1:10	1:25	1:20	1:15	1:10
$\theta_{\gamma}$ (°)	19.31	19.41	19.52	19.63	19.63	19.72	19.83	19.91
$\theta_{002}$ (°)	23.50	23.62	23.94	24.12	23.61	23.81	23.80	24.01
$\theta_{100}$ (°)	44.62	44.70	45.43	45.24	44.70	45.30	45.43	44.82
$d_m$ (Å)	3.77	3.74	3.74	3.70	3.78	3.76	3.73	3.70
$d_r$ (Å)	5.66	5.62	5.61	5.57	5.73	5.71	5.68	5.66
$L_a$ (Å)	17.55	16.51	15.67	15.25	16.09	15.98	14.90	14.21
$L_c$ (Å)	9.75	9.38	8.88	8.53	9.17	8.98	8.73	8.34
$M_e$	3.58	3.50	3.38	3.31	3.44	3.40	3.33	3.25
$R_a$	6.58	6.19	5.88	5.72	6.03	5.99	5.59	5.33
$f_{a-XRD}$	0.61	0.60	0.58	0.58	0.45	0.43	0.42	0.40

$$^a f_{a-XRD} = A_{002} / (A_{\gamma} + A_{002}).$$

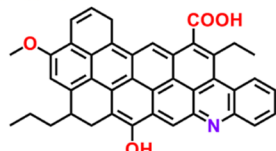
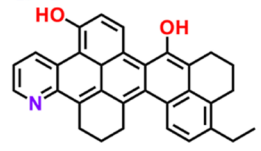
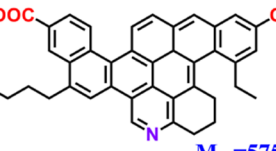
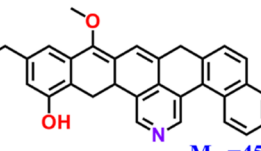
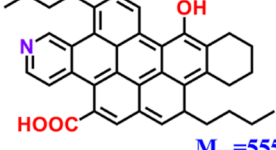
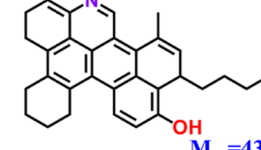

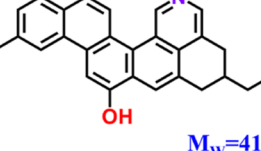
more significant  $\pi$ - $\pi$  accumulation. Siddiqui et al.<sup>48</sup> have suggested that XRD detection is capable of indicating the aromaticity of heavy fractions ( $f_{a-XRD}$ ), i.e., in accordance with the area of  $\gamma$  peak and 002 peak. With the elevation of the COR, the number of the catalytic active sites was increased, and the aromatic ring saturation reaction was intensified. Thus, the  $f_{a-XRD}$  value tended to decline, and the value of asphaltene was significantly higher than that of resin, consistent with the previous research results, suggesting the reliability of the XRD analysis results.

**3.7. Prediction of the Average Molecular Structure Model.** The basic carbon skeleton structure was determined according to the average molecular formula in Table 3 and a series of structural parameters in Table S1. Subsequently, the average molecular structure model of heavy fractions at different CORs was reasonably predicted according to the occurrence forms of characteristic functional groups and heteroatoms obtained by FT-IR and XPS, as presented in Figure 10.

## 4. CONCLUSIONS

In this study, the composition structure and hydrogenation conversion law of heavy fractions in coal tar were explored by various characterization methods based on new separation method. The chemical composition and microstructure of heavy fractions of coal tar before and after hydrogenation are obtained from a new perspective, especially the rare studied resin, which will be of great significance to the further use of coal tar with high added value and the development of coal chemical industry.

The following important conclusions were drawn: (1) with the increase of the COR, the formation rate of resin from primary asphaltene was less than that of resin from primary asphaltene converted into the aromatic content, such that the resin content declined, while the content of asphaltene was reduced sharply. The contents of heteroatomic elements and  $M_w$  of heavy fractions tended to decline. (2) The lightness reaction led to the reduction of the intensity of characteristic peaks of hydrogen bond group and aromatic C-H in FT-IR spectra, whereas the intensity of aliphatic C-H was increased.

COR	Asphaltene	Resin
1:25	$C_{41}H_{31}O_4N$  $M_w=601.23$	$C_{32}H_{27}O_2N$  $M_w=457.20$
1:20	$C_{40}H_{33}O_3N$  $M_w=575.25$	$C_{32}H_{29}O_2N$  $M_w=459.22$
1:15	$C_{38}H_{37}O_3N$  $M_w=555.28$	$C_{31}H_{31}ON$  $M_w=433.24$
1:10	$C_{38}H_{37}O_2N$  $M_w=539.28$	$C_{30}H_{29}ON$  $M_w=419.22$

**Figure 10.** Prediction chart of average molecular structure of heavy fractions at different CORs.

The aromatic rings and total rings of heavy fractions were reduced. Likewise, the above-mentioned values of asphaltene were greater than those of resin, whereas the parameters were greater than those of asphaltene. (3) The content of  $sp^2$  hybrid carbon with aromatic ring structure declined, whereas the aliphatic  $sp^3$  hybrid carbon was increased. Compared with resin, asphaltene exhibited smaller  $d_m$  and  $d_r$ , and higher  $L_a$ ,  $L_c$ ,  $M_a$ , and  $R_a$ , corresponding to its structure with a higher degree of condensation. The above-mentioned six crystallization parameters tended to decline with the increase of the COR.

The research on the composition and structure of coal tar and hydrogenation process in this paper can guide the separation of coal tar components, the improvement of hydrogenation process and the design of catalyst, and guide the transformation of coal tar utilization technology to low carbon emission and high value-added chemicals at the molecular level.

## ASSOCIATED CONTENT

### Supporting Information

The Supporting Information is available free of charge at <https://pubs.acs.org/doi/10.1021/acsomega.3c00032>.

Attribution and chemical shift of proton types in the molecular structure model, XPS survey spectra of heavy fractions under different COR, and types and distribution of hydrogen atoms in heavy fractions under different COR (PDF)

## AUTHOR INFORMATION

### Corresponding Authors

**Yang Yang** – School of Chemical Engineering, The Research Center of Chemical Engineering Applying Technology for Resource of Shaanxi, Northwest University, Xi'an, Shaanxi 710069, China; Email: [alextoyang@163.com](mailto:alextoyang@163.com)

**Dong Li** – School of Chemical Engineering, The Research Center of Chemical Engineering Applying Technology for Resource of Shaanxi, Northwest University, Xi'an, Shaanxi 710069, China; [orcid.org/0000-0002-4578-0595](https://orcid.org/0000-0002-4578-0595); Email: [lidong@nwu.edu.cn](mailto:lidong@nwu.edu.cn)

### Authors

**Yi Wang** – School of Chemical Engineering, The Research Center of Chemical Engineering Applying Technology for Resource of Shaanxi, Northwest University, Xi'an, Shaanxi 710069, China

**Feng Tian** – School of Chemical Engineering, The Research Center of Chemical Engineering Applying Technology for Resource of Shaanxi, Northwest University, Xi'an, Shaanxi 710069, China

**Yonghong Zhu** – School of Chemical Engineering, The Research Center of Chemical Engineering Applying Technology for Resource of Shaanxi, Northwest University, Xi'an, Shaanxi 710069, China; Hydrocarbon High-Efficiency Utilization Technology Research Center, Yanchang Petroleum Co. Ltd., Xi'an, Shaanxi 710075, China

**Louwei Cui** – Northwest Research Institute of Chemical Industry Co., Ltd., Xi'an, Shaanxi 710061, China

Xiaoyong Fan – School of Chemistry and Chemical Engineering, Yulin University, Yulin, Shaanxi 719000, China

Chongpeng Du – School of Chemical Engineering, The Research Center of Chemical Engineering Applying Technology for Resource of Shaanxi, Northwest University, Xi'an, Shaanxi 710069, China

Feili Wang – School of Chemical Engineering, The Research Center of Chemical Engineering Applying Technology for Resource of Shaanxi, Northwest University, Xi'an, Shaanxi 710069, China

Huanan Zheng – School of Chemical Engineering, The Research Center of Chemical Engineering Applying Technology for Resource of Shaanxi, Northwest University, Xi'an, Shaanxi 710069, China

Complete contact information is available at:  
<https://pubs.acs.org/10.1021/acsomega.3c00032>

## Notes

The authors declare no competing financial interest.

## ACKNOWLEDGMENTS

We gratefully acknowledge the financial support of the National Natural Science Foundation of China (21978237), Shaanxi Technology Innovation Shaanxi Key Research and Development Plan Project (2018zdxm-gy-161), Natural Science Basic Research Program of Shaanxi (2021JLM-19), Natural Science Basic Research Program of Shaanxi (2019JLP-03), Innovation Capability Support Program of Shaanxi (2020TD-028), and Science and Technology Plan of Yulin Government (CXY-2020-002-07).

## REFERENCES

- (1) Menghu, Y.; Feng, Y.; Miao, C. Production operation countermeasures of crude oil sequential processing in the new situation. *Pet. Refin. Eng.* **2020**, *50*, 20–24.
- (2) Yuan, Y.; Li, D.; Zhang, L.-N.; Zhu, Y.-H.; Wang, L.; Li, W. Development, status, and prospects of coal tar hydrogenation technology. *Energy Technol.* **2016**, *4*, 1338–1348.
- (3) Xu, J.; Yang, Y.; Li, Y.-W. Recent development in converting coal to clean fuels in China. *Fuel* **2015**, *152*, 122–130.
- (4) Stratiev, D.; Shishkova, I.; Ivanov, M.; Dinkov, R.; Georgiev, B.; Argirov, G.; Atanassova, V.; Vassilev, P.; Atanassov, K.; Yordanov, D.; et al. Catalytic cracking of diverse vacuum residue hydrocracking gas oils. *Chem. Eng. Technol.* **2021**, *44*, 997–1008.
- (5) Li, D.; Cui, W.-G.; Zhang, X.-P.; Meng, Q.-H.; Zhou, Q.-C.; Ma, B.-Q.; Niu, M.-L.; Li, W.-H. Production of clean fuels by catalytic hydrotreating a low temperature coal tar distillate in a pilot-scale reactor. *Energy Fuels* **2017**, *31*, 11495–11508.
- (6) Yu, H.; Li, S.-Y.; Jin, G.-Z. Catalytic hydrotreating of the diesel distillate from Fushun shale oil for the production of clean fuel. *Energy Fuels* **2010**, *24*, 4419–4424.
- (7) Liu, J.; Cui, L.-W.; Fan, X.-Y.; Xu, X.; Shi, J.-H.; Tian, J.-Y.; Li, D. Effect of adding graphene oxide on the structure and properties of needle coke. *J. Anal. Appl. Pyrolysis* **2021**, *160*, 105329.
- (8) Du, J.-T.; Deng, W.-N.; Li, C.; Zhang, Z.-L.; Yang, T.-F.; Guo, R.-L. Reactivity and structure changes of coal tar asphaltene during slurry-phase hydrocracking. *Energy Fuels* **2017**, *31*, 1858–1865.
- (9) Du, C.-P.; Li, D.; Shi, C.; Du, Z.-G.; Han, W.; Zhu, Y.-H.; Dong, H.; Fan, X.-Y.; Wang, C. Study on the association driving force of low temperature coal tar asphaltene. *J. Mol. Struct.* **2022**, *1254*, 132361.
- (10) Zhu, Y.-H.; Du, C.-P.; Zheng, H.-A.; Wang, F.-L.; Tian, F.; Liu, X.; Li, D. Molecular representation of coal-derived asphaltene based on high resolution mass spectrometry. *Arabian J. Chem.* **2022**, *15*, 103531.
- (11) Zuo, P.-P.; Qu, S.-J.; Shen, W.-Z. Asphaltene: Separations, structural analysis and applications. *J. Energy Chem.* **2019**, *34*, 186–207.
- (12) Chacón-Patiño, M.-L.; Rowland, S.-M.; Rodgers, R. P. Advances in asphaltene petroleomics. Part 1: Asphaltene are composed of abundant island and archipelago structural motifs. *Energy Fuels* **2017**, *31*, 13509–13518.
- (13) Chacón-Patiño, M.-L.; Rowland, S.-M.; Rodgers, R. P. Advances in asphaltene petroleomics. Part 2: Selective separation method that reveals fractions enriched in island and archipelago structural motifs by mass spectrometry. *Energy Fuels* **2018**, *32*, 314–328.
- (14) Chacón-Patiño, M.-L.; Rowland, S. M.; Rodgers, R. P. Advances in asphaltene petroleomics. Part 3: Dominance of island or archipelago structural motif is sample dependent. *Energy Fuels* **2018**, *32*, 9106–9120.
- (15) Chacón-Patiño, M.-L.; Smith, D.-F.; Hendrickson, C.-L.; Marshall, A.-G.; Rodgers, R.-P. Advances in asphaltene petroleomics. Part 4: Compositional trends of solubility subfractions reveal that polyfunctional oxygen containing compounds drive asphaltene chemistry. *Energy Fuels* **2020**, *34*, 3013–3030.
- (16) Zhu, Y.-H.; Zheng, H.-A.; Tian, F.; Wang, Y.-J.; Huang, C.-F.; Dan, Y.; Yang, T.; Du, N.; Zhou, Q.-C.; Li, D. Characterization of nitrogen-containing compounds in coal tar and its subfractions by comprehensive two-dimensional GC×GC-TOF and ESI FT-ICR mass spectrometry based on new separation method. *Fuel Process. Technol.* **2022**, *227*, 107125.
- (17) Zhu, Y.-H.; Guo, Y.-T.; Teng, H.-P.; Liu, J.; Tian, F.; Cui, L.-W.; Li, W.; Liu, J.-J.; Wang, C.; Li, D. Analysis of oxygen-containing species in coal tar by comprehensive two-dimensional GC×GC-TOF and ESI FT-ICR mass spectrometry through a new subfraction separation method. *J. Energy Inst.* **2022**, *101*, 209–220.
- (18) Yun, W.; Xieqing, W.; Zhiguo, W.; Pengfei, W.; Weiping, W.; Liang, Z. Comparison of molecular composition and structure of asphaltene from coal tar and vacuum residue. *Acta Pet. Sin., Pet. Process. Sect.* **2019**, *35*, 303–311.
- (19) Zhu, Y.-H.; Tian, F.; Liu, Y.-Q.; Cui, L.-W.; Dan, Y.; Du, C.-P.; Li, D. Comparison of the composition and structure for coal-derived and petroleum heavy subfraction by an improved separation method. *Fuel* **2021**, *292*, 120362.
- (20) Mosio-Mosiewski, J.; Morawski, I. Study on single-stage hydrocracking of vacuum residue in the suspension of Ni–Mo catalyst. *Appl. Catal., A* **2005**, *283*, 147–155.
- (21) Morawski, I.; Mosio-Mosiewski, J. Effects of parameters in Ni–Mo catalysed hydrocracking of vacuum residue on composition and quality of obtained products. *Fuel Process. Technol.* **2006**, *87*, 659–669.
- (22) Pei, L.-J.; Li, D.; Liu, X.; Cui, W.-G.; Shao, R.-T.; Xue, F.-F.; Li, W.-H. Investigation on asphaltene structures during low temperature coal tar hydrotreatment under various reaction temperatures. *Energy Fuels* **2017**, *31*, 4705–4713.
- (23) Shao, R.-T.; Shen, Z.-W.; Li, D.; Sun, Z.-H.; Pei, L.-J.; Liu, X.; Li, W.-H.; Dan, Y. Investigation on composition and structure of asphaltene during low-temperature coal tar hydrotreatment under various reaction pressures. *J. Anal. Appl. Pyrolysis* **2018**, *136*, 44–52.
- (24) Jin, N.; Wang, G.; Han, S.; Meng, Y.-M.; Xu, C.-M.; Gao, J.-S. Hydroconversion behavior of asphaltene under liquid-phase hydrogenation conditions. *Energy Fuels* **2016**, *30*, 2594–2603.
- (25) Wang, L.-Y.; Wang, Q.; Liu, Y.-Q.; Yao, Q.-X.; Sun, M.; Ma, X.-X. Catalytic conversion of asphaltene to BTXN using metal-loaded modified HZSM-5. *Chin. J. Chem. Eng.* **2022**, *49*, 253–264.
- (26) Zhu, Y.; Guo, Y.-T.; Zhang, X.; Tian, F.; Luo, C.; Du, C.; Yang, T.; Chen, M.; Sun, Z.; Li, D. Exploration of coal tar asphaltene molecules based on high resolution mass spectrometry and advanced extraction separation method. *Fuel Process. Technol.* **2022**, *233*, 107309.
- (27) Petrochemical industry standard of the people's Republic of China. *Test method for separation of asphalt into four fractions*. NB/SH/T 0509-2010; National Energy Administration of China, 2010.

- (28) Han, Z.-X.; Sun, Y.-D.; Yang, Z.-H. Influence of initial hydrogen pressure on asphaltene hydroconversion. *Pet. Process. Petrochem.* **2014**, *45*, 21–24.
- (29) Zhang, H.-C.; Yan, Y.-J.; Qi, B.-F.; Sun, W.-F. Study on the nitrogen distribution and removal during residue hydrotreating. *Pet. Process. Petrochem.* **2007**, *38*, 43–46.
- (30) Zhang, H.-C.; Yan, Y.-J.; Sun, W.-F.; Dai, Y.-C. Distribution and removal of sulfur during hydrotreating of residue. *J. Fuel Chem. Technol.* **2007**, *35*, 628–631.
- (31) Liu, J.; Tian, F.; Liu, J.-P.; Guo, Q.; Fan, X.-Y.; Dan, Y.; Fu, Q.-J.; Du, Z.-G.; Han, W.; Song, D.; Li, D. Structure Characterization and solubility analysis of the existent gum of the Fischer-Tropsch synthetic crude. *ACS Omega* **2020**, *5*, 18778–18786.
- (32) Sun, Z.-H.; Li, D.; Ma, H.-X.; Tian, P.-P.; Li, X.-K.; Li, W.-H.; Zhu, Y.-H. Characterization of asphaltene isolated from low-temperature coal tar. *Fuel Process. Technol.* **2015**, *138*, 413–418.
- (33) Fattahi Mehraban, M.; Farzaneh, S.-A.; Sohrabi, M. Functional compounds of crude oil during low salinity water injection. *Fuel* **2021**, *285*, 119144.
- (34) Kang, Y.-H.; Wei, X.-Y.; Li, J.; Jin, H.-T.; Li, T.; Lu, C.-Y.; Ma, X.-R.; Zong, Z.-M. Green and effective catalytic hydroconversion of an extractable portion from an oil sludge to clean jet and diesel fuels over a mesoporous Y zeolite-supported nickel catalyst. *Fuel* **2021**, *287*, 119396.
- (35) Xiong, G.; Li, Y.-S.; Jin, L.-J.; Hu, H.-Q. In situ FT-IR spectroscopic studies on thermal decomposition of the weak covalent bonds of brown coal. *J. Anal. Appl. Pyrolysis* **2015**, *115*, 262–267.
- (36) Mullins, O.-C. The asphaltenes. *Annu. Rev. Anal. Chem.* **2011**, *4*, 393–418.
- (37) Dickie, J.-P.; Yen, T.-F. Macrostructures of the asphaltic fractions by various instrumental methods. *Anal. Chem.* **1967**, *39*, 1847–1852.
- (38) Gabrienko, A.-A.; Martyanov, O.-N.; Kazarian, S.-G. Effect of temperature and composition on the stability of crude oil blends studied with chemical imaging in situ. *Energy Fuels* **2015**, *29*, 7114–7123.
- (39) Kang, Y.-H.; Wei, X.-Y.; Liu, G.-H.; Gao, Y.; Li, Y.-J.; Ma, X. R.; Zhang, Z. F.; Zong, Z. M. Catalytic hydroconversion of soluble portion in the extraction from Hecaogou subbituminous coal to clean liquid fuel over a Y/ZSM-5 composite zeolite-supported nickel catalyst. *Fuel* **2020**, *269*, 117326.
- (40) Furimsky, E. Catalytic hydrodeoxygenation. *Appl. Catal., A* **2000**, *199*, 147–190.
- (41) Du, J.-T.; Zhang, D.-K.; Zhang, M.-X.; Jia, H. N.; Nie, Y.; Sun, Y. K.; Deng, W. A.; Li, C. Structure characteristics and association behavior of coal and petroleum C7-asphaltene. *J. Fuel Chem. Technol.* **2020**, *48*, 674–682.
- (42) Zhu, X.; Zhu, Z.; Han, C. Quantitative determination of oxygen-containing functional groups in coal by FTIR spectroscopy. *J. Fuel Chem. Technol.* **1999**, *27*, 335–339.
- (43) Xie, K. C. *Coal structure and its reactivity*; Science Press: Beijing, China, 2002.
- (44) Induchoodan, G.; Jansson, H.; Swenson, J. Influence of graphene oxide on asphaltene nanoaggregates. *Colloids Surf., A* **2021**, *630*, 127614.
- (45) Geng, W.; Kumabe, Y.; Nakajima, T.; Takanashi, H.; Ohki, A. Analysis of hydrothermally-treated and weathered coals by X-ray photoelectron spectroscopy (XPS). *Fuel* **2009**, *88*, 644–649.
- (46) Yonghong, Z.; Jiangliu, H.; Yong, D.; Lei, W.; Wenhong, L.; Dong, D. Analysis and characterization of medium/low temperature coal tar asphaltene. *Acta Pet. Sin., Pet. Process. Sect.* **2016**, *32*, 334–342.
- (47) Bouhadda, Y.; Bormann, D.; Sheu, E.; Bendedouch, D.; Krallafa, A.; Daou, M. Characterization of Algerian Hassi-Messaoud asphaltene structure using Raman spectrometry and X-ray diffraction. *Fuel* **2007**, *86*, 1855–1864.
- (48) Siddiqui, M.-N.; Ali, M.-F.; Shirokoff, J. Use of X-ray diffraction in assessing the aging pattern of asphalt fractions. *Fuel* **2002**, *81*, 51–58.